A New Harmonic Current Control Approach of Dual Three-phase PMSM in Degraded Mode

Wenjing Zhang[2] weijing.zhang@ensam.eu

Ngac Ky Nguyen[1] ngacky.nguyen@ensam.eu

Eric Semail[1] eric.semail@ensam.eu

Yanliang Xu[2] xuyanliang@sdu.edu.cn

[1]*Univ. Lille, Arts et Metiers Institute of Technology, Centrale Lille, Yncrea Hauts-de-France, ULR 2697 - L2EP, F-59000 Lille, France*

[2]*School of Electrical Engineering, Shandong University, China*

***Abstract*— This paper presents a new approach to control properly the currents of a dual three-phase PMSM operating in open-circuit fault condition with a wide speed range. Using fault tolerant control strategies proposed in the literature lead to high frequency current components in the rotor frame. Operating at high speed required in some industrial applications induces a strong constraint on the current controllers. In this paper, a second transformation matrix resulting constant currents in the new frame is proposed. However, there is still a coupling between axes. Thus, a simple Adaptive Linear Neuron is proposed to decouple and enhance the performance of the current tracking. Comparative simulation results are shown for a 12slots/8poles dual three-phase PMSM to confirm the validity of the proposed method.**

Keywords—dual three-phase PMSM, multiphase fault tolerance control, Adaline, new transformation matrix, harmonic current control (HCC), multi-reference frame (MRF), open phase

NOMENCLATURE

$i_{pd}, i_{pq}, i_{nd}, i_{nq}$	Current in *pd-pq* and *nd-nq* frames under healthy condition
θ	Electrical angle of rotor
$i_{pd,f}, i_{pq,f}, i_{nd,f}, i_{nq,f}$	Phase current in *pd-pq* and *nd-nq* frames under fault condition
T_{em}	Electromagnetic torque
$I_{pq,0}, I_{pq,2}$	Amplitude of constant and second harmonic components of i_{pq}
$u_{pd}, u_{pq}, u_{nd}, u_{nq}$	Phase voltage in *pd-pq* and *nd-nq* frames
$u_{A1}, u_{B1}, u_{C1}, u_{A2}, u_{B2}, u_{C2}$	Phase voltage in natural frame
n	Rotation speed of electric machine (r/min)
$i_{pd,0}, i_{pq,0}, i_{nd,0}, i_{nq,0}$	Constant component of phase current in *pd-pq* and *nd-nq* frames under fault condition
$i_{pd,2}, i_{pq,2}, i_{nd,2}, i_{nq,2}$	Second harmonic component of phase current in *pd-pq* and *nd-nq* frames under fault condition
$\vec{i}_{p,0}$	DC vector consisting of $i_{pd,0}$ and $i_{pq,0}$
$\vec{i}_{p,h2}$	Second harmonic current vector consisting of $i_{pd,2}$ and $i_{pq,2}$
$\vec{i}_{p,A}, \vec{i}_{p,B}$	Current vector in *pAd-pAq* frame and *pBd-pBq* frame
A_p, B_p	Magnitude of $\vec{i}_{p,A}$ and $\vec{i}_{p,B}$
k_r	Resonant gain
ω_c	Cut-off frequency
ω_{pr}	Reference angular frequency
σ	Sharpness of the notch filter
$i_{DC1}, i_{DC2}, i_{DC3}, i_{DC4}$	Phase current in *DC1-DC2* and *DC3-DC4* frames
μ_1, μ_2	Weights of ADALINE
η	Learning rate
y_{err}	Error between the reference and feedback SMRF current

I. INTRODUCTION

Taking a consideration of compromise between the complexity and fault tolerant performances, the Dual Three-phase Permanent Magnet Synchronous Machine (DT-PMSM) is the most promising structure [1]. The mathematical model and control method of DT-PMSM are more closed to that of conventional three-phase PMSM. Besides, the minimum order of its torque ripple is up to 12th while it is 6th in three-phase PMSM resulting in a low torque ripple.

The ability to operate smoothly under fault condition is the most important characteristic of DT-PMSM assuring its high functional reliability. The constraint of a constant torque of DT-PMSM under open-circuit fault condition leads to the necessity of the reconfiguration of the reference currents [2]. The latter can be reconfigured in the rotor frame by which the transformation matrices are consistent for both normal and fault conditions leading to the unchanged mathematical model for Fault Tolerant Control (FTC). Thus, it benefits from the advantages of high accuracy and simple implementation and has been developed in amounts of studies [2], [3]. However, the harmonic components will be introduced into the reference current after the reconfiguration by FTC [2]. The PI controllers are generally used for the control of these reference currents. Due to alternating current (AC) components, it inevitably leads to a phasor delay between actual and reference values [4]. This issue can be ignored while electric machine operates under low speed, but it gradually worsens as the increase of speed and eventually impacts the smoothness of output torque. Thus, most studies about the FTC of DT-PMSM generally proceed the simulations and experiments below a restrained speed that limits the dynamic performance of drive system under fault condition [5], [6].

Therefore, it is essential to ensure that the reference current of FTC for DT-PMSM can be tracked well even under high-speed condition to achieve the smooth torque output under an expanded Speed Operation Range (SOR). And the effect of the track for reference current of FTC is mainly

influenced by the regulation for the harmonic components. Thus, the harmonic current control (HCC) method is crucial for improving the accessible SOR of DT-PMSM under fault condition. The most common HCC methods mainly rely on multi-reference frame (MRF) or proportional-resonant controller (PR) [7], [8]. MRF is firstly proposed in [9] where it is used to track three-phase reference currents with arbitrary balanced harmonic content. In [10], the harmonic components in d-q frame are transformed into a pair of positive and negative sequence harmonic vectors and the relative rotating harmonic reference frames based on the basic Park transformation are used to map the rotating harmonic vector in d-q frame to invariant vectors in harmonic reference frames. Eventually, the control for the AC components is simplified to the control of direct current (DC) components. In [11], MRF is used in HCC of DT-PMSM under fault condition. The FTC current vectors in two decoupled reference frames are transformed into DC components using MRF, respectively. However, three times the number of PI controllers are required compared to previous control method without MRF leading to the increase of the calculation burden. Alternatively, using PR in HCC of DT-PMSM is easier for implementation. PR is mainly characterized by the excellent track ability for the AC component [12]. In [13], a modified quasi-PR controller is used for HCC of DT-PMSM under fault condition. However, the tuning parameters of PR controller need to be adaptively modulated according to the actual speed in order to ensure the control performance [10] specially in transient operations. Besides, there are no related studies that report the comparison of performances between different HCC methods used for FTC of DT-PMSM.

This paper investigates the FTC of DT-PMSM and its HCC with expanded SOR to reduce the torque ripple of DT-PMSM under fault and high-speed condition. The rest of this paper is organized as follows. Firstly, the mathematical model and FTC strategy of DT-PMSM is derived. Then, different HCC methods are investigated for the FTC of DT-PMSM. Except for the previously proposed MRF and PR methods, a novel simplified MRF method compensated by ADAptive LInear NEuron (SMRF-ADALINE) is proposed to achieve the HCC of DT-PMSM under fault condition while the compromise between the calculation complexity and control accuracy is considered. Finally, the FTC control performances for the DT-PMSM under high speed of aforementioned HCC methods are compared via the simulation.

II. FTC OF DT-PMSM

In this paper, a DT-PMSM with 30 electrical degrees shift, separated neutral points and surface-mounted rotor PMs is considered. The neutral points of two 3-phase winding sets are separated.

It is supposed that an open-phase fault occurs in the phase A2. To deal with this fault, the switch components powering for phase A2 is disabled. It can be realized that the relationship of the currents in healthy 3-phase winding (A1-B1-C1) can be remained while it is changed in another fault 3-phase winding (A2-B2-C2) under fault condition. The reconfigured current in decoupled frame can be calculated as shown in (1) [2].

The parameters of the prototype are shown in Table I. The schematic diagram of FTC strategy for prototype DT-PMSM is shown in Fig. 1.

$$\begin{cases} i_{pd,f} = \dfrac{I_{pq,2}}{2}\sin\left(2\theta - \dfrac{\pi}{6}\right) \\ i_{pq,f} = \dfrac{I_{pq,0} + I_{pq,2}}{2} \\ i_{nd,f} = \dfrac{I_{pq,0} - I_{pq,2}}{2} + I_{pq,2}\cos\left(2\theta + \dfrac{5\pi}{6}\right) \\ i_{nq,f} = \dfrac{I_{pq,2}}{2}\sin\left(2\theta - \dfrac{\pi}{6}\right) \end{cases} \tag{1}$$

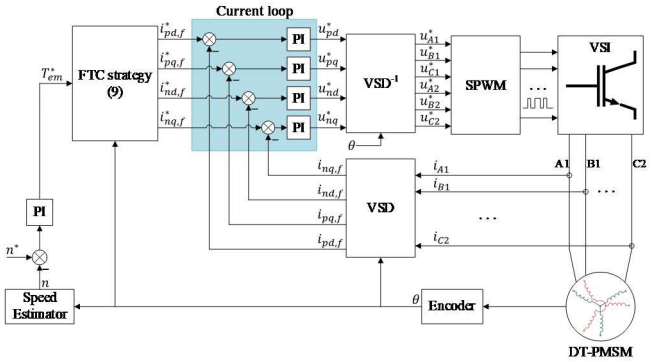

Fig. 1. Control block diagram of FTC for prototype DT-PMSM.

TABLE I. PARAMETERS OF THE PROTOTYPE

Parameter	Symbol	Value
Rated power	P_N	2.15kW
Rated speed	n_m	1500rpm
Rated torque	T_N	13.6N·m
Rated current	I_N	3.87A
Rated voltage	U_N	210V
Number of pole pairs	p	4
Winding resistance	R_s	0.7Ω
Inductance in *pd-pq* frame	L_{pd} and L_{pq}	7.7mH
Inductance in *nd-nq* frame	L_{nd} and L_{nq}	8.3mH

III. HCC OF FTC

It can be seen from (1) that the second harmonics exist in the reconfigured current under fault condition. However, the traditional PI controller cannot achieve the accurate control for the AC component [14], especially under high-speed condition. Therefore, some HCC methods aiming at the reconfigured current of FTC for DT-PMSM is investigated in this paper including the MRF method, PR method and SMRF-ADALINE method.

A. MRF method

The reference current in FTC (1) can be further decomposed into DC component and second harmonic component.

The PI controller is directly used to regulate the DC component. In terms of the control of the second harmonic component, the MRF method is utilized and the *pd-pq* frame is demonstrated here as an example. The schematic diagram of the MRF transformation in the *pd-pq* frame is shown in Fig. 2. $\vec{i}_{p,0}$ is the DC vector consisting of $i_{pd,0}$ and $i_{pq,0}$ while $\vec{i}_{p,h2}$ denotes the second harmonic current vector consisting of $i_{pd,2}$ and $i_{pq,2}$. *pAd-pAq* and *pBd-pBq* denote the frames rotating in positive or negative sequence with respect to the *pd-pq* frame at twice the electrical angular speed, respectively. $\vec{i}_{p,h2}$ can be furtherly expressed as a composite of the current vector $\vec{i}_{p,A}$ in *pAd-pAq* frame and $\vec{i}_{p,B}$ in *pBd-pBq* frame:

$$\vec{i}_{p,h2} = \vec{i}_{p,A} + \vec{i}_{p,B} = A_p e^{j(2\theta+\varphi_A)} + B_p e^{-j(2\theta+\varphi_B)} \quad (2)$$

where A_p and B_p represent the magnitude of $\vec{i}_{p,A}$ and $\vec{i}_{p,B}$, respectively.

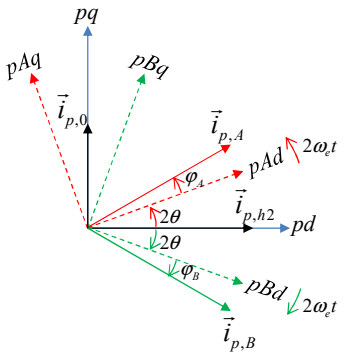

Fig. 2. Schematic diagram of MRF transformation.

By applying the Park transformation at $e^{-j2\theta}$ and the Park inverse transformation at $e^{j2\theta}$, $\vec{i}_{p,A}$ and $\vec{i}_{p,B}$ can be transformed to the invariant vector in the *pAd-pAq* frame and *pBd-pBq* frame. Finally, the control for the $\vec{i}_{p,h2}$ is transformed to the control of constant vectors. Fig. 3 shows the control block diagram of MRF method that replaces the current loop section in Fig. 1.

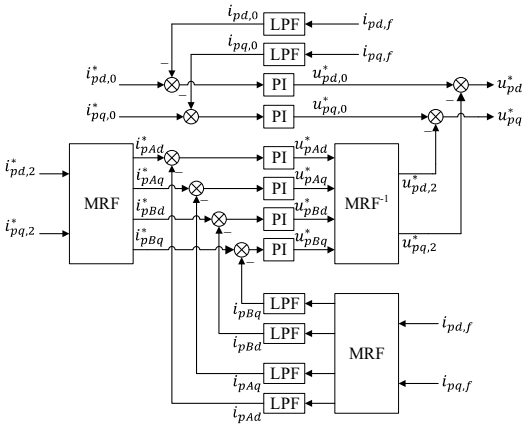

Fig. 3. Block diagram of current loop using MRF method (*pd-pq* frame).

It can be seen from Fig. 3 that there are 6 PI current controllers and 6 low pass filters (LPF) used for the HCC in the *pd-pq* frame. Thus, there are totally 12 PI controllers and 12 LPF to achieve the HCC of DT-PMSM under fault condition (1 phase opened) increasing the complexity for real-time implementation.

B. PR method

It can be seen from Fig. 3 that the number of PI controllers is much more compared with the previous current loop in Fig. 1. Alternatively, PR method is easier to implement which requires fewer controllers in current loop. PR controllers possess a distinctive resonant loop, enabling them to track high frequency AC signals. The transfer function of the PR controller is as follows:

$$G_{PR} = k_P + \frac{k_r \omega_c s}{s^2 + 2\omega_c s + \omega_{pr}^2} \quad (3)$$

Where k_r is the resonant gain, ω_c is the cut-off frequency, and ω_{pr} is the reference angular frequency which needs to be adjusted in real time with the variance of speed.

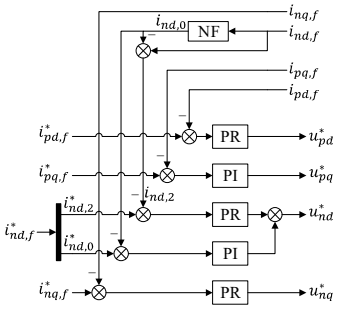

Fig. 4. Block diagram of current loop using PR method.

The block diagram of PR method for FTC of DT-PMSM is shown in Fig. 4. It can be seen that the second harmonics in (1) is controlled by PR controller while the DC components are still modulated by previous PI controllers.

It is worth to notice that $i_{nd,f}$ only contains the second harmonic component that can be eliminated using a notch filter (NF). The transfer function of NF is as follows [15]:

$$H(s) = \frac{s^2 + \omega_c^2}{s^2 + \sigma s + \omega_c^2} \quad (4)$$

where ω_c is the band-stop frequency and σ is the sharpness of the filter.

C. SMRF-ADALINE method

According to the reconfigured current given in (1), the second harmonic components can also be expressed as follows:

$$\begin{cases} i_{pd,f} = \dfrac{I_{pq,2}}{2}\sin\left(2\theta - \dfrac{\pi}{6}\right) \\ i_{nd,2} = -I_{pq,2}\cos\left(2\theta - \dfrac{\pi}{6}\right) \\ i_{nq,f} = \dfrac{I_{pq,2}}{2}\sin\left(2\theta - \dfrac{\pi}{6}\right) \end{cases} \quad (5)$$

It can be found that the regularities existing in (5) could be beneficial for the simplification and transformation to DC components. Firstly, a constant coefficient matrix as shown in (6) is used to modify the equations in (5) with the same amplitude. Then, the PARK transformation matrix (7) in terms of $\left(2\theta - \pi/6\right)$ is used to achieve the transformation to the DC components.

$$\mathbf{P}_{cc} = \begin{bmatrix} 1 & 0 \\ 0 & \dfrac{1}{2} \end{bmatrix} \quad (6)$$

$$\mathbf{P}_{park} = \begin{bmatrix} \cos\left(2\theta - \dfrac{\pi}{6}\right) & \sin\left(2\theta - \dfrac{\pi}{6}\right) \\ -\sin\left(2\theta - \dfrac{\pi}{6}\right) & \cos\left(2\theta - \dfrac{\pi}{6}\right) \end{bmatrix} \quad (7)$$

Finally, the current components in *pd-nd-nq* frame as given in (5) can be transformed into the DC components in

novel SMRF (*DC1-DC2* and *DC3-DC4*). The transformation to the SMRF is shown as follows:

$$\begin{bmatrix} i_{DC1} \\ i_{DC2} \end{bmatrix} = \mathbf{P}_{park}\mathbf{P}_{cc}\begin{bmatrix} i_{pd} \\ i_{nd,2} \end{bmatrix} = \begin{bmatrix} 0 \\ -\dfrac{I_{pq,2}}{2} \end{bmatrix} \tag{8}$$

$$\begin{bmatrix} i_{DC3} \\ i_{DC4} \end{bmatrix} = \mathbf{P}_{park}\mathbf{P}_{cc}\begin{bmatrix} i_{nq} \\ i_{nd,2} \end{bmatrix} = \begin{bmatrix} 0 \\ -\dfrac{I_{pq,2}}{2} \end{bmatrix} \tag{9}$$

The block diagram of SMRF method is shown in Fig. 5. However, it should be noted that the existence of $\mathbf{P}_{cc}$ leads to the coupling between i_{DC1} and i_{DC2} (i_{DC3} and i_{DC4}) which increases the complexity of the design of the controllers. The influence of the coupling on the SMRF current is investigated as shown in Fig. 6(a) when the switches of ADALINE are off. The load torque is set to 10N·m and the operation speed is set under 1500r/min. Additionally, the impact of SPWM is neglected. It can be found that there is second harmonic component in SMRF currents which results from the coupling.

In order to eliminate the harmonic component in SMRF current as shown in Fig. 6(a), ADALINE is introduced to compensate the coupling between i_{DC1} and i_{DC2} (i_{DC3} and i_{DC4}) as shown in Fig. 5 when the switches are all closed. The internal structure of ADALINE used in SMRF-ADALINE method is shown in Fig. 7 in which only the second harmonic is considered. The weights μ_1 and μ_2 are updated based on the principle of least mean square (LMS):

$$\begin{aligned} \mu_1(k+1) &= \mu_1(k) + \eta y_{err}(k)\cos(2\theta) \\ \mu_2(k+1) &= \mu_2(k) + \eta y_{err}(k)\sin(2\theta) \end{aligned} \tag{10}$$

where η is the learning rate; y_{err} is the error between the reference and feedback SMRF current.

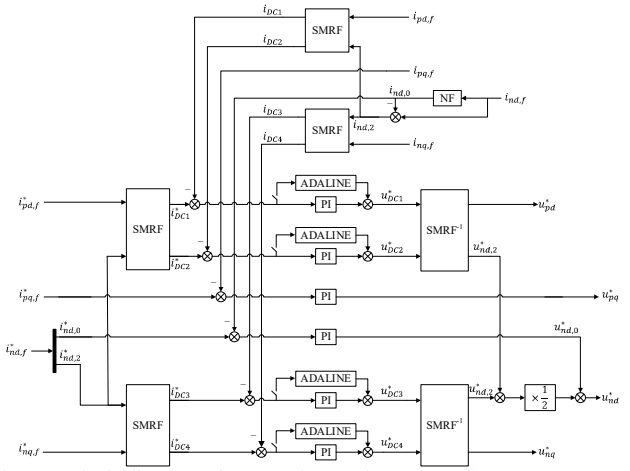

Fig. 5. Block diagram of current loop using SMRF (SMRF-ADALINE) method.

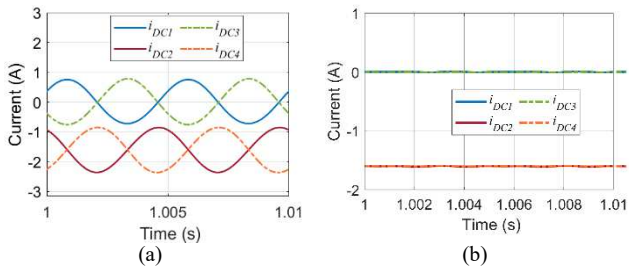

Fig. 6. Influence of the coupling on SMRF currents: (a) Without using ADALINE. (b) After using ADALINE.

The learning rate η mainly depends on the sampling time of control system and the characteristics of tracked current [16]. It is mandatory to set η between 0 and 1 for the stability of control system. Generally, higher learning rate means faster convergence speed while it induces instability of system. A more detailed discussion on η is given in [16]. In this paper, η is set to 0.02.

The SMRF current while the switches in Fig. 5 are closed is shown in Fig. 6(b). It can be concluded that the coupling in SMRF is compensated well using ADALINE.

In summary, the SMRF-ADALINE method consists of 6 PI controllers and 4 ADALINE compensators (having the same structure) while only one NF is used to separate the DC and harmonic components in $i_{nd,f}$.

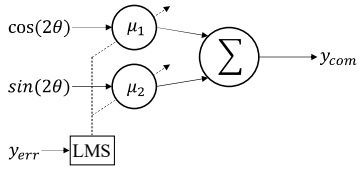

Fig. 7. Schematic diagram of ADALINE [16].

IV. Simulation Results and Comparison

A. Effectiveness Validation of HCC Methods

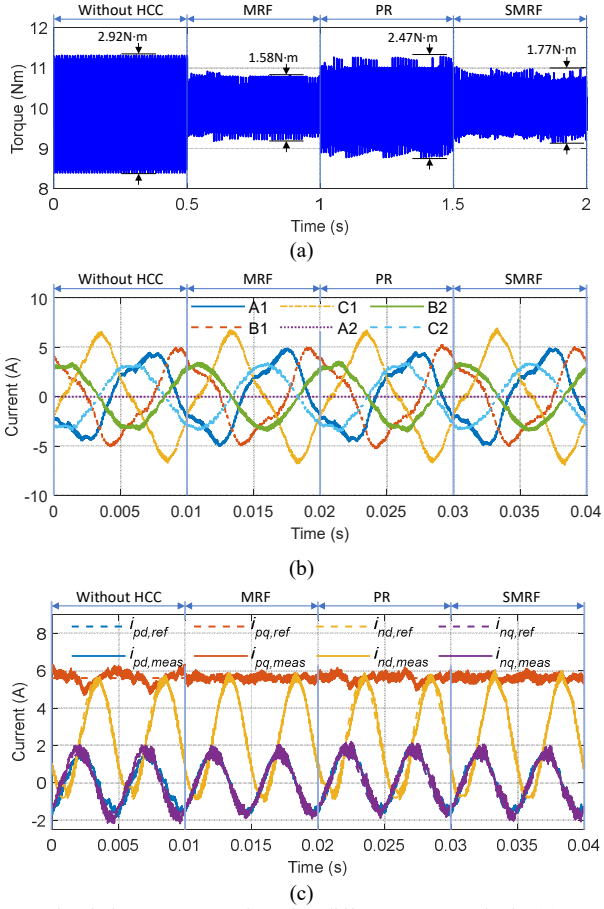

Fig. 8. Simulation current results using different HCC methods: (a) Torque waveform (b) Phase current waveform. (c) Decoupled current waveform (1500rpm).

In order to validate and compare the performance of different HCC methods,

Fig. 8 shows the simulation results using different HCC methods under FTC condition at 1500 rpm. The change of the torque waveform is given in Fig. 8(a) while the reference torque is set to 10N·m. It can be seen that the utilization of HCC method effectively suppresses the torque fluctuation under high-speed FTC condition. The torque ripple is reduced from 29.2% to 15.8% and 17.7% using MRF and SMRF, respectively while it is only reduced to 24.7% using PR method.

Fig. 8(b) shows the phase winding current waveforms switching into different HCC methods. And the decoupled current in dual d-q frame is shown in

Fig. 8(c) which is actually tracked by designed HCC methods. It can be seen that the tracking performance can be significantly improved by using MRF and SMRF methods. The current waveforms shown in Fig. 8(c) are analyzed using Fast Fourier Transform (FFT).

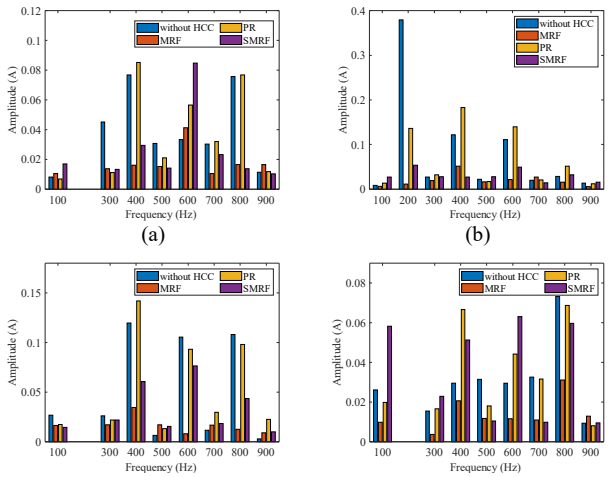

Fig. 9. Harmonic analysis and comparison of current waveforms in decoupled frame: (a) $i_{pd,f}$. (b) $i_{pq,f}$. (c) $i_{nd,f}$. (d) $i_{nq,f}$.

B. Dynamic Performance under Speed Change

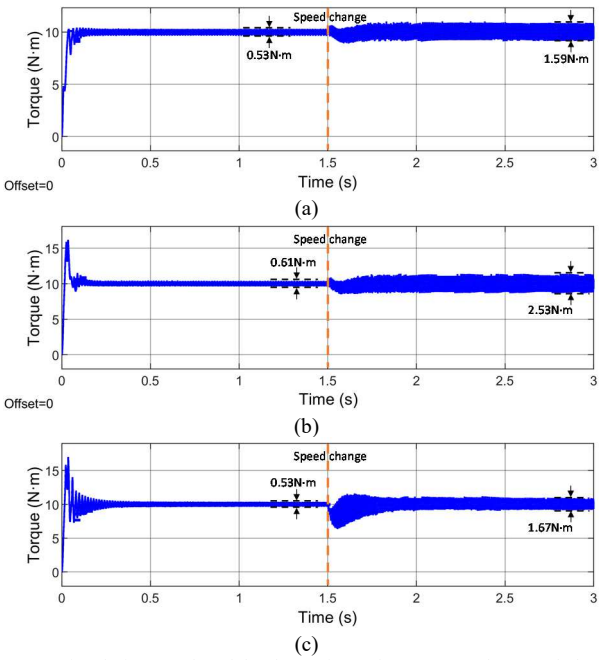

Fig. 10. Simulation results of the dynamic performance under speed change: (a) Variance of torque using MRF method. (b) Variance of torque using PR method. (c) Variance of torque using SMRF-ADALINE method.

The comparison of harmonic components except the effective parts as given in (1) between the current waveforms obtained by different HCC methods is shown in Fig. 9. It can be seen that the harmonic suppression effect of MRF method is prominent, followed by SMRF method.

Fig. 10 compares the dynamic torque performance under speed change condition while the reference torque is still set to 10N·m. As shown in Fig. 10(a), the speed changes from 500 rpm to 1500 rpm. From Fig. 10(b)-(d), it can be seen that the torque ripple is nearly same under 500 rpm using all three HCC methods. However, there is the obvious difference under 1500 rpm where torque fluctuation using MRF and SMRF is nearly same while it is much higher using PR method. In SMRF method, adaptive neural network-ADALINE is used to compensate the second harmonic resulting from the coupling.

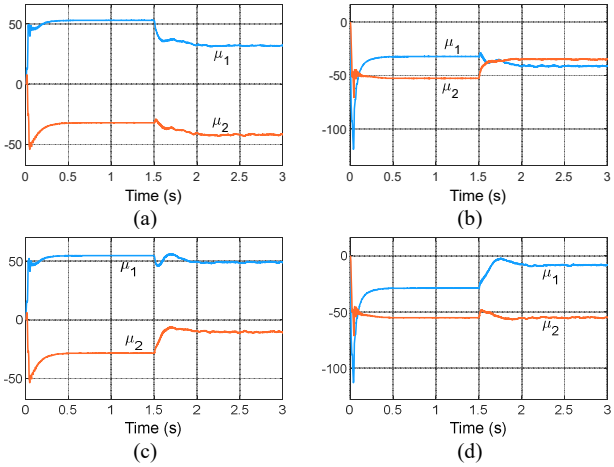

Fig. 11. Iteration of the weights in SMRF-ADALINE method during speed change: (a) iDC1. (b) iDC2. (c) iDC3. (d) iDC4. (η=0.02)

C. Dynamic Performance under Torque Change

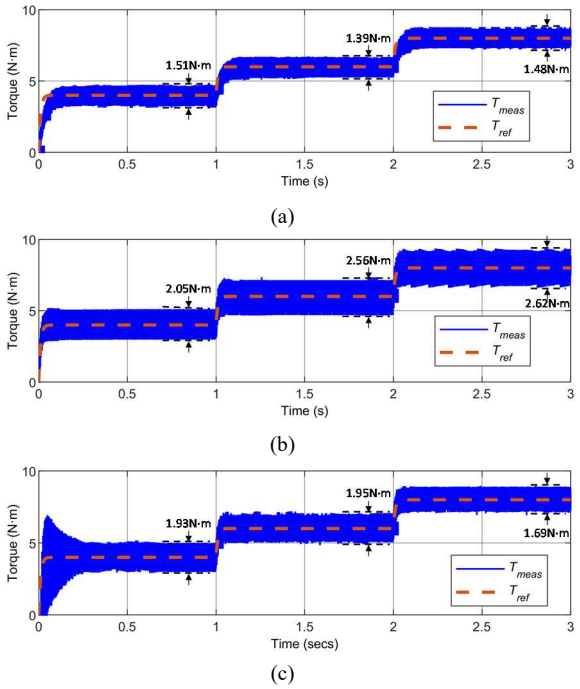

Fig. 12. Simulation results of the dynamic performance under torque change: (a) MRF method. (b) PR method. (c) SMRF-ADALINE method.

The iterative processes of weights in each ADALINE are shown in Fig. 11 and the learning rate is set to 0.02. It can be

seen that the convergence process is short that is suitable for the practical application. Fig. 12 compares the dynamic performance under the torque change condition in which the torque is set to 4 N·m at the beginning, increases to 6 N·m at 1s and furtherly increases to 8 N·m at 2s. The speed is set to 1500 rpm. It can be seen that the torque ripple is nearly equal during the total torque change dynamic process through the utilization of MRF while it gradually deteriorates using PR method. In the case of SMRF method, the torque fluctuation remains unchanged below 6 N·m and decreases while the torque increases to 8 N·m. It can be concluded that the dynamic performance of MRF method under torque change is prominent while it performs worst using PR method.

The iterative processes of weights in each ADALINE during torque change condition are shown in Fig. 13. We can observe that the convergence is guaranteed after each change.

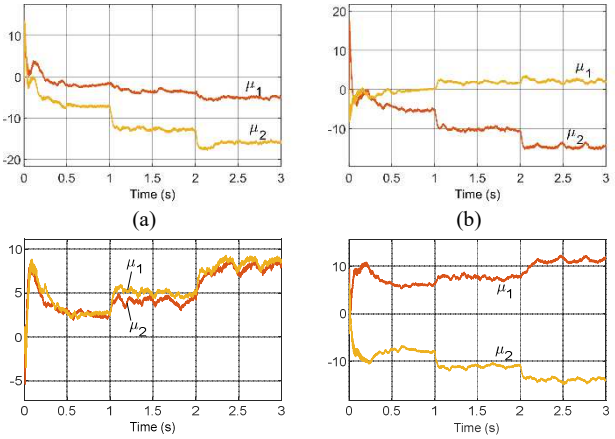

Fig. 13. Iteration of the weights in SMRF-ADALINE method during torque change: (a) i_{DC1}. (b) i_{DC2}. (c) i_{DC3}. (d) i_{DC4}. (η=0.02)

V. CONCLUSION

In this paper, HCC methods of FTC for DT-PMSM are investigated to extend SOR under fault condition. The main contributions include the proposition of SMRF method based on the novel transformation matrix as well as ADALINE and the comparative research of different HCC methods. The comparisons of the control block diagram are summarized in both Table II and Table III.

TABLE II. COMPARISON OF THE CONTROL BLOCK DIAGRAM - I

	PI		PR		ADALINE		Total	
	Num	TP	Num	TP	Num	TP	Num	TP
MRF	12	2	0	3	0	1	12	24
PR	2		3		0		5	13
SMRF	6		0		4		10	13

Num: Number of controllers in each method. TP: Number of tuning parameters in each controller.

TABLE III. COMPARISON OF THE CONTROL BLOCK DIAGRAM – II

	Num of LPF	Num of NF
MRF	12	0
PR	0	1
SMRF	0	1

TABLE IV. COMPARISON OF TORQUE PERFORMANCE UNDER HIGH-SPEED FTC CONDITION

	Torque Fluctuation (N·m)				
Speed (rpm)	500	1500			
Ref torque (N·m)	10	4	6	8	10
MRF	0.53	1.51	1.39	1.48	1.59
PR	0.61	2.05	2.56	2.62	2.53
SMRF	0.53	1.93	1.95	1.69	1.67

Based on above comparisons, the main results are summarized as follows.

a) MRF method features the highest level of complexity that combines 12 controllers, 24 TPs and 12 LPFs while it can be significantly reduced by use of PR and SMRF methods resulting in less calculation burden.

b) The torque ripple of both MRF and SMRF methods is nearly same and PR method presents a highest value .

c) The torque fluctuation is nearly same under 500 rpm for all three HCC methods. The torque fluctuation of MRF is lowest under 1500 rpm while it is worst using PR method.

REFERENCES

[1] Y. Zhao and T. A. Lipo, "Space vector PWM control of dual three-phase induction machine using vector space decomposition," IEEE Trans Ind Appl, vol. 31, no. 5, pp. 1100–1109, 1995.

[2] G. Feng, C. Lai, W. Li, J. Tjong, and N. C. Kar, "Open-phase fault modeling and optimized fault-tolerant control of dual three-phase permanent magnet synchronous machines," IEEE Trans Power Electron, vol. 34, no. 11, pp. 11116–11127, 2019.

[3] G. Feng, C. Lai, W. Li, Y. Han, and N. C. Kar, "Computation-efficient solution to open-phase fault tolerant control of dual three-phase interior PMSMs with maximized torque and minimized ripple," IEEE Trans Power Electron, vol. 36, no. 4, pp. 4488–4499, 2020.

[4] H. Guzman et al., "Comparative study of predictive and resonant controllers in fault-tolerant five-phase induction motor drives," IEEE Transactions on Industrial Electronics, vol. 63, no. 1, pp. 606–617, Jan. 2016, doi: 10.1109/TIE.2015.2418732.

[5] P. Shi, X. Wang, X. Meng, M. He, Y. Mao, and Z. Wang, "Adaptive Fault-Tolerant Control for Open-Circuit Faults in Dual Three-Phase PMSM Drives," IEEE Trans Power Electron, pp. 1–12, 2022, doi: 10.1109/TPEL.2022.3223411.

[6] W. Wang, J. Zhang, M. Cheng, and S. Li, "Fault-Tolerant Control of Dual Three-Phase Permanent-Magnet Synchronous Machine Drives Under Open-Phase Faults," IEEE Trans Power Electron, vol. 32, no. 3, pp. 2052–2063, Mar. 2017, doi: 10.1109/TPEL.2016.2559498.

[7] J. Qu, J. Jatskevich, C. Zhang, and S. Zhang, "Torque ripple reduction method for permanent magnet synchronous machine drives with novel harmonic current control," IEEE Transactions on Energy Conversion, vol. 36, no. 3, pp. 2502–2513, Sep. 2021, doi: 10.1109/TEC.2021.3056557.

[8] Z. Zhong, S. Zhou, and Z. Shao, "Multiple reference frame-based current harmonic control for interior PMSMs considering motional EMF," Journal of Power Electronics, vol. 21, no. 6, pp. 921–931, Jun. 2021, doi: 10.1007/s43236-021-00238-4.

[9] P. L. Chapman and S. D. Sudhoff, "A multiple reference frame synchronous estimator/regulator," IEEE Transactions on energy conversion, vol. 15, no. 2, pp. 197–202, 2000.

[10] G. Feng, C. Lai, J. Tian, and N. C. Kar, "Multiple reference frame based torque ripple minimization for PMSM drive under both steady-state and transient conditions," IEEE Trans Power Electron, vol. 34, no. 7, pp. 6685–6696, 2018.

[11] G. Feng, C. Lai, W. Peng, and N. C. Kar, "Decoupled Design of Fault-Tolerant Control for Dual-Three-Phase IPMSM with Improved Memory Efficiency and Reduced Current RMS," IEEE Transactions on Transportation Electrification, vol. 8, no. 1, pp. 1144–1154, Mar. 2022, doi: 10.1109/TTE.2021.3091468.

[12] H. Cha, T.-K. Vu, and J.-E. Kim, "Design and control of Proportional-Resonant controller based Photovoltaic power conditioning system," in 2009 IEEE Energy Conversion Congress and Exposition, IEEE, 2009, pp. 2198–2205.

[13] B. Zheng, J. Zou, B. Li, M. Tang, Y. Xu, and P. Zanchetta, "Analysis and Fault-Tolerant Control for Dual-Three-Phase PMSM Based on Virtual Healthy Model," IEEE Trans Power Electron, vol. 37, no. 12, pp. 15411–15424, Dec. 2022, doi: 10.1109/TPEL.2022.3199100.

[14] D. Bao, X. Pan, and Y. Wang, "A Novel Hybrid Control Method for Single-Phase-Input Variable Frequency Speed Control System with a Small DC-Link Capacitor," IEEE Trans Power Electron, vol. 34, no. 9, pp. 9016–9032, Sep. 2019, doi: 10.1109/TPEL.2018.2890000.

[15] I. Jeong, B. J. Hyon, and K. Nam, "Dynamic modeling and control for SPMSMs with internal turn short fault," IEEE Trans Power Electron, vol. 28, no. 7, pp. 3495–3508, 2013, doi: 10.1109/TPEL.2012.2222049.

[16] D. T. Vu, N. K. Nguyen, and E. Semail, "Fault-tolerant control for nonsinusoidal multiphase drives with minimum torque ripple," IEEE Trans Power Electron, vol. 37, no. 6, pp. 6290–6304, 2021.